Dear author,

Please note that changes made in the online proofing system will be added to the article before publication but are not reflected in this PDF.

We also ask that this file not be used for submitting corrections.

Solid State Nuclear Magnetic Resonance xxx (xxxx) xxx

Contents lists available at ScienceDirect

Solid State Nuclear Magnetic Resonance

journal homepage: www.elsevier.com/locate/ssnmr

Direct dynamic nuclear polarization of ^{15}N and ^{13}C spins at 14.1 T using a trityl radical and magic angle spinning

ARTICLE INFO

Keywords
MAS-DNP
Trityl OX063
AMUPol
Direct polarization
Cross polarization
Solid effect
Cross effect

ABSTRACT

We investigate solid-state dynamic nuclear polarization of ^{13}C and ^{15}N nuclei using monoradical trityl OX063 as a polarizing agent in a magnetic field of 14.1 T with magic angle spinning at ~100 K. We monitored the field dependence of direct ^{13}C and ^{15}N polarization for frozen [^{13}C, ^{15}N] urea and achieved maximum absolute enhancement factors of 240 and 470, respectively. The field profiles are consistent with polarization of ^{15}N spins via either the solid effect or the cross effect, and polarization of ^{13}C spins via a combination of cross effect and solid effect. For microcrystalline, ^{15}N-enriched tryptophan synthase sample containing trityl radical, a 1500-fold increase in ^{15}N signal was observed under microwave irradiation. These results show the promise of trityl radicals and their derivatives for direct polarization of low gamma, spin-½ nuclei at high magnetic fields and suggest a novel approach for selectively polarizing specific moieties or for polarizing systems which have low levels of protonation.

1. Introduction

Solid-State NMR is a powerful method to obtain structural information at the atomic level but the breadth of its applications is restricted by its inherent low sensitivity. Studying chemical species with low concentration and/or isotopes at natural abundance levels is often impractical due to time consuming signal averaging. To circumvent these limitations, dynamic nuclear polarization (DNP), combined with magic angles spinning (MAS), appears to be a powerful approach. MAS-DNP has enabled studies that would have been otherwise impossible, ranging from catalyst surfaces [1–6], to proteins under biologically relevant conditions [7–13], to samples with NMR active isotopes at low natural abundance [14–19].

DNP transfers the higher electron polarization from a polarizing agent (PA) to the surrounding nuclei by irradiating with an appropriate microwave (MW) frequency. The MAS-DNP experiment consists of spinning the sample at low temperature (typically ~100 K) and irradiating it with a high power MW source [20,21]. The most efficient PAs are biradicals [22], which enhance the proton polarization via the Cross Effect (CE) mechanism [23,24]. Proton polarization is subsequently transferred to the targeted nuclei via cross-polarization [25]. This method is particularly powerful and can, under certain circumstances, be applied to samples with a low proton content [26–28]. Extensive work has been carried out to improve the efficiency of PAs [29–33] or to adjust their affinity to the target [34–37]. Nonetheless the overall sensitivity can remain low. This becomes especially challenging at high magnetic field due to the experimental [32,38–41] and theoretical dependencies of the DNP mechanisms [23,39,42,43].

For many samples, direct polarization of the targeted nuclei is attractive vs. cross-polarization from ^{1}H, specifically for observing low gamma nuclei which are not protonated due to either the inherent chemistry of the moiety of interest or because the sample has been extensively deuterated to mitigate relaxation effects. This approach, commonly used for dissolution DNP, has found some applications for MAS-DNP [44–52]. Recently Corzilius et al. have probed the efficiency of Gd and bis-Gd chelates to directly polarize ^{13}C and ^{15}N under biological conditions [46,53]. Following their work, we report here the first high field (14.1 T) study of trityl OX063 to directly polarize ^{13}C and ^{15}N under biologically relevant conditions.

In this article, we present enhancement of ^{13}C and ^{15}N spin polarization as a function of the main magnetic field (the DNP enhancement profile) using a model sample to illustrate the mechanisms at stake. We measure the polarization gains corrected by bleaching losses and depolarization factor as well as the polarization build-up times and MW power dependence. Additionally, we demonstrate the use of trityl OX063 to directly enhance an ^{15}N-enriched protein sample and show that high sensitivity can be achieved by directly polarizing ^{15}N spins to achieve SNR on par with the standard DNP approach using AMUPol and cross-polarization (CP) [29], with unprotonated ^{15}N moieties exhibiting a relatively larger enhancement by direct polarization.

2. Materials and methods

2.1. Urea samples

Three samples containing equal volumes of 2 M [^{13}C, ^{15}N] urea in D_8-glycerol/D_2O/H_2O (60/30/10; v/v/v) were prepared. The first contained 40 mM trityl OX063 (Oxford Instruments Molecular Biotools), the second contained 20 mM trityl OX063, and the third was radical-free. The same 3.2 mm sapphire MAS rotor was used to characterize these samples.

2.2. Tryptophan synthase samples

U-^{15}N tryptophan synthase (TS) was expressed and purified as

https://doi.org/10.1016/j.ssnmr.2019.03.009
Received 7 February 2019; Received in revised form 27 March 2019; Accepted 28 March 2019
Available online xxxx

previously described [54,55]. TS microcrystals were crystallized by 1:1 dilution of the soluble protein with 50 mM bicine in D_2O, pH adjusted to 7.8 with CsOH, containing 14% PEG-8000 (W/V) and 3 mM spermine. Crystals were harvested at 10,000 rpm for 10 minutes at 4 °C and washed with bicine buffer in 90% D_2O, pH adjusted to 7.8 with CsOH, containing 1.5 mM spermine, 8% PEG-8000 (W/V), 10% DMSO (V/V) and an excess of the high-affinity α-site ligand N-(4′-trifluoro-methoxybenzenesulfonyl)-2-amino-ethyl phosphate (F9). Microcrystals were again harvested at 10,000 rpm for 10 minutes at 4 °C and loaded into 3.2 mm sapphire MAS rotors with a sample volume of ~25 μL; rotors were packed to identical levels using a single batch of microcrystals in an attempt to match the amount of protein in each rotor. Radical, either AMUPol or trityl OX063, was added directly to the samples in the rotors from concentrated stock solutions made using the same crystallization buffer to achieve a final radical concentration of 20 mM for AMUPol and 20 mM and 40 mM for trityl OX063.

2.3. Simulation of trityl EPR line shape

The simulated EPR spectrum of trityl OX063 at 14.1 T was obtained using EasySpin [56]. We assumed a g-tensor with principle components [g_{xx}, g_{yy}, g_{zz}] [2.003193 2.003193 2.002583] [57] and linebroadening of 1 mT Gaussian and 1mT Lorentzian. These parameters were based on literature values for the g-tensor [57] and our prior experimental measurements of trityl OX063 EPR spectra at 240 GHz.

2.4. NMR/DNP measurements for urea samples

NMR and DNP measurements were carried out on a custom DNP NMR system operating at 14.1 T with a 395 GHz gyrotron described in detail elsewhere [58]. Reported MW powers were measured at the input to the MAS probe with an Ophir 3A-P-THz pyrometer calibrated by comparison with an absorbing water load. All [^{13}C, ^{15}N] urea spectra were collected at 7 kHz MAS. Direct (DPMAS) ^{15}N and ^{13}C polarization NMR spectra were obtained via a π/2 excitation pulse centered at the resonance of interest with ~100 kHz proton decoupling during signal acquisition. To measure absolute sensitivity, spectra were collected for both ^{13}C and ^{15}N using the radical-free sample with a recycle delay of $3T_{1n}$ to calculate the maximum achievable thermally polarized signal. Microwave power was optimized under conditions where efficient DNP was expected for the trityl radical, and DNP enhancement profiles for ^{13}C and ^{15}N were collected by varying the main magnetic field while holding the gyrotron frequency at 395.175 GHz. For each field measurement, the nuclear excitation and monitoring frequencies were set on resonance. Recycle delays were set to 300 s and 200 s for ^{13}C and ^{15}N measurements, respectively, and saturation pulse trains on both ^{1}H and ^{13}C/^{15}N channels destroyed any existing polarization prior to DNP buildup. For measurements of absolute maximum DNP enhancement, DNP buildup measurements, in which polarization is measured as a function of delay between saturation pulses and a π/2 excitation pulse, were performed at field positions for maximum ^{13}C and ^{15}N direct polarization. The ratios of maximum signal intensities for the MW-on experiments for the trityl-containing samples and the MW-off experiments for the radical-free sample, scaled by the number of scans for each spectrum, were used to estimate the absolute sensitivity enhancements. The absolute enhancement provides an assessment of the combined effects of depolarization under MAS and any trityl bleaching of nearby nuclear spins in order to provide an evaluation of the real gain by direction polarization from electrons to ^{13}C and ^{15}N using 40 mM trityl OX063 [40] (also called θ [59]). This measurement of absolute enhancement was used to scale the relative enhancements measured at other magnetic field settings.

2.5. NMR/DNP measurements for tryptophan synthase (TS) samples

All TS spectra were collected at 10 kHz MAS. DPMAS ^{15}N spectra for the trityl OX063 containing samples were obtained via a π/2 excitation pulse at the resonance of interest with ~100 kHz proton decoupling during signal acquisition. Cross polarization magic-angle spinning (CPMAS) ^{15}N spectra for the AMUPol containing sample were obtained via a π/2 excitation pulse on the proton channel followed by 2 msec of ^{15}N cross polarization before ~100 kHz proton decoupling during signal acquisition. CPMAS spectra were not attempted for the trityl containing samples as proton measurements on [^{13}C, ^{15}N] urea samples showed little DNP enhancement. Similarly, DPMAS spectra were not collected for the AMUPol containing sample as direct polarization of ^{15}N from AMUPol is not as efficient as DNP of ^{1}H followed by cross polarization. For measurements of relative DNP enhancement of ^{15}N, DNP buildup measurements, in which polarization is measured as a function of delay between saturation pulses and the π/2 excitation pulse, were performed for the trityl- and AMUPol-containing TS samples. Trityl-containing samples were measured at a field position for maximum ^{15}N polarization by the trityl monoradical using DPMAS and the AMUPol-containing sample was measured at a field position for maximum ^{1}H polarization by the AMUPol biradical using CPMAS. The ratios of maximum achievable signal intensities for the DPMAS and CPMAS experiments for the trityl-containing and AMUPol-containing samples, respectively, were scaled by the number of scans for each spectrum and the relative time needed for polarization buildup to calculate the sensitivity per unit time for the different radicals.

3. Results and discussion

3.1. Field dependence for ^{15}N and ^{13}C polarization

Direct ^{15}N and ^{13}C polarization measurements of [^{13}C, ^{15}N] urea by 40 mM trityl OX063 as a function of external magnetic field are shown in Fig. 1 along with a simulated EPR spectrum for the trityl radical. The FWHM of the simulated Trityl OX063 EPR lineshape is 4.37 mT. The difference in magnetic fields corresponding to the ^{15}N enhancement maxima is 4.26 mT. The ^{15}N Larmor frequency at this field corresponds to 2.17 mT. Thus, the solid effect (SE) mechanism for ^{15}N enhancement would predict maximal enhancements separated by 4.34 mT while the CE mechanism would predict a separation of 2.17 mT. Given the inherent broadening due to the spin properties of the trityl radical, the observed polarization enhancement profile for ^{15}N is consistent with either mechanism of polarization transfer since the positive and negative maximal enhancements occur within the EPR line shape at about twice the ^{15}N Larmor frequency [47]. The enhancement profile for ^{13}C polarization is more complex and consistent with polarization via a combination of the SE and the CE [47,60] since the maxima are separated by almost twice the ^{13}C Larmor frequency, or 10.77 mT, and are well beyond the limits of EPR line shape. We also measured ^{1}H polarization, but found only a 14-fold polarization enhancement via the trityl radical, as would be expected for narrow line radical polarizing via the SE.

3.2. Achievable maximum ^{15}N and ^{13}C polarization

DNP theoretical gains for ^{15}N and ^{13}C are 6500 and 2620, respectively, for ideal transfer of polarization when compared to equilibrium thermal polarization. Measurements of ^{15}N and ^{13}C polarization using 40 mM trityl OX063 at an optimal field setting and comparing microwaves on vs microwaves off spectra yield gains of 2510 and 530, respectively (Table 1). However, comparison to a control sample, which contains no radical, indicates absolute gains of 470 and 240, respectively, implying that ^{15}N and ^{13}C signal are significantly attenuated by bleaching and/or depolarization under MAS by the high concentration of trityl OX063 required to achieve significant DNP. It is unlikely that a further improvement could be achieved by decreasing the radical concentration to reduce bleaching/depolarization as measurements using a sample containing 20 mM trityl OX063 showed significantly less bleaching and/or depolarization but also substantially lower DNP enhancement. The optimal microwave power needed for maximum polarization

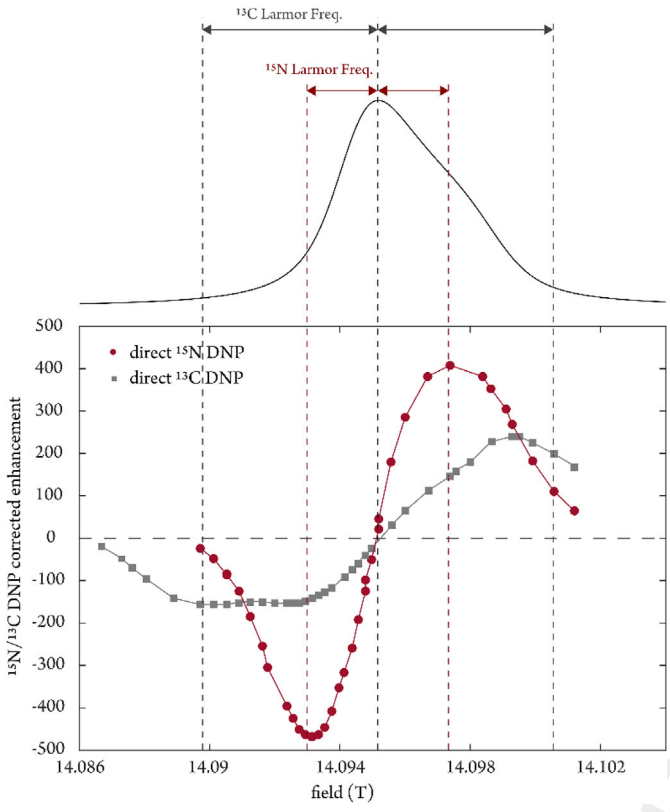

Fig. 1. ^{15}N and ^{13}C absolute enhancement as a function of magnetic field for 2 M [^{13}C,^{15}N]urea in glycerol-d_8–D_2O–H_2O (60 : 30: 10 vol ratio) containing 40 mM OX063 trityl radical at 98 K and a MAS spinning rate of 7 kHz. Lines between points are provided to guide the eye and are not a fit of the data. The gyrotron frequency was fixed at 395.175 GHz. For each magnetic field setting, ^{15}N and ^{13}C absolute enhancements were measured via direct polarization by comparing NMR signal with and without microwaves using a 300 s (^{15}N) or 200 s (^{13}C) buildup time and considering the signal reduction caused by the presence of trityl. For reference, a simulated EPR spectrum of trityl at 14.095 T is provided.

Table 1
^{15}N and^{13}C maximum DNP enhancements for 2 M^{13}C-^{15}N-urea in glycerol-d_8–D_2O–H_2O (60 : 30: 10 vol ratio) containing 40 mM and 20 mM OX063 trityl radical at 98 K and a MAS spinning rate of 7 kHz. DNP enhancement values were calculated considering signal reduction caused by the presence of trityl.

trityl conc./mM	40			20		
	$\varepsilon_{on/off}$	$\varepsilon_{Depol} \times \varepsilon_{Bleaching}$	ε_{abs}	$\varepsilon_{on/off}$	$\varepsilon_{Depol} \times \varepsilon_{Bleaching}$	ε_{abs}
^{15}N	2510	0.19	470	220	0.43	94
^{13}C	530	0.45	240	–	–	–

enhancement using trityl OX063 was similar to the optimal power for AMUPol (Fig. 2). We note that ^{15}N DNP enhancement via the trityl radical builds more quickly at lower power levels, consistent with it having a narrower field profile. This suggests an alternative strategy for applications of DNP which are power limited (i.e. when using MW sources with lower power output, such as klystrons [61–63]). At the temperatures needed for DNP, the ^{15}N and ^{13}C T_1 relaxation times for frozen urea are quite long at 3026 s and 1869 s (Table 2), respectively, for the radical-free sample. They only decrease to 1676 s and 905 s, respectively, in the presence of 40 mM trityl OX063, leading to very long DNP buildup times. In an attempt to shorten the polarization buildup time, a [^{13}C, ^{15}N] urea sample containing both 40 mM trityl OX063 and 4 mM Gd-fullerene was also tested (data not shown). The addition of Gd-fullerene reduced the DNP buildup time by shortening ^{13}C and ^{15}N T_1 relaxation rates without any observable further reduction in thermal

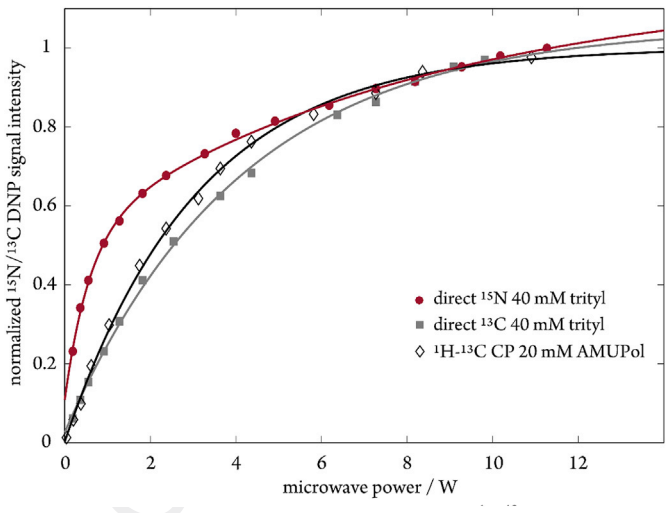

Fig. 2. Power dependence of DNP enhancement for ^{1}H-^{13}C CPMAS (open diamonds), ^{13}C DPMAS (solid squares), and ^{15}N DPMAS (solid circles) for 2 M [^{13}C-^{15}N]urea samples containing either 20 mM AMUPol (CPMAS) or 40 mM trityl OX063 (DPMAS) with a glassing matrix of glycerol-d8–D_2O–H_2O (60:30:10 vol ratio) at 98 K and 7 KHz MAS rate. Plotted lines are simple functions provided to guide the eye. Power measurements were collected at the main magnetic fields corresponding to the maximal DNP enhancements for each approach.

Table 2
Polarization buildup times for 2 M^{13}C-^{15}N-urea in glycerol-d_8–D_2O–H_2O (60: 30: 10 vol ratio) containing 40 mM OX063 trityl radical and for an undoped sample at 98 K and a MAS spinning rate of 7 kHz.

trityl conc./mM		40	0
^{15}N[a]	mw on	1251	–
	mw off	1284	1869
^{13}C[b]	mw on	1078	–
	mw off	905	3026

[a] NMR field at 14.09326 T (negative maximum^{15}N enhancement).
[b] NMR field at 14.09964 T (positive maximum^{13}C enhancement).

Table 3
Signal-to-noise comparison for^{15}N spectra of^{15}N-enriched Tryptophan synthase collected using CPMAS and 20 mM AMUPol vs DPMAS and 40 mM trityl. Spectra acquired at 14.1 T with 10 kHz MAS at 98 K. Input mw power was set to 11 W at 395.175 GHz.

experiment/sample	SNR per time unit	DNP buildup times/s (ratios)
DPMAS/40 mM trityl	1.6	41, 681 (1:2)
DPMAS/20 mM trityl	0.9	38, 636 (1:6)
CPMAS/20 mM AMUPol	1.0	–

equilibrium polarization for either ^{13}C or ^{15}N. However, DNP enhancements were also reduced due to shortening the T_{1e} relaxation rate of the trityl radical. A lower concentration (e.g. $\leq$ 1 mM) of Gd-fullerene or a similar compound may sufficiently shorten the nuclear spin relaxation rates without deleteriously affecting the trityl T_{1e} relaxation rate, but we have not extensively tested its concentration dependence (see Table 3). Q2

DNP buildup, depolarization and absolute enhancement for Tryptophan Synthase (TS).

To test the viability of direct ^{15}N polarization using trityl OX063 in a protein sample, we measured the DNP polarization for a microcrystalline ^{15}N-enriched TS sample. We note that for this protein we have found that cryoprotectants and crystallization conditions utilized for characterizing this protein by diffraction at low temperature (e.g. 10% DMSO and 8% PEG-8000 [64]) also work well for keeping the AMUPol biradical well

distributed for the purposes of DNP. To evaluate trityl OX063 polarization relative to typical conditions for proteins, we also prepared a sample containing 40 mM trityl OX063 and a control sample containing 20 mM AMUPol (i.e. a sample with the same e^- spin concentration but using a proven biradical PA). We first characterized the optimal DNP power needed for polarizing with 40 mM trityl OX063 and the DNP buildup time (Fig. 3). The power needed for optimal polarization was similar to the power needed for optimal polarization using 20 mM AMUPol. DNP buildup curves observed for for 20 mM OX063 trityl and 40 mM trityl OX063 containing samples were very similar and consistently biexponential with a fast component having a DNP buildup time of 38–41 s and a slow component exhibiting a buildup time of 636–681 s. However, the ratio of the fast and slow components altered from 1:6 with 20 mM trityl OX063 to 1:2 with 40 mM trityl OX063, consistent with an increase in radical concentration. We note that the bimodal buildup behavior can be explained via several possible mechanisms. The first is that there are two populations of trityl radicals—one which is evenly distributed and solvated with a second population existing in an aggregated form; this would agree with the differences we observe with radical concentration. A second possibility is that polarization of the microcrystals proceeds via an inefficient spin diffusion process since the ^{15}N spin bath is very weakly coupled due to its substantially lower gyromagnetic ratio relative to ^{1}H [43,65–67]. A third possibility is that some of the microcrystalline protein is dissolving into the surrounding buffer. While we did not observe any loss of crystals and maintained the buffer reagents at a constant concentration to minimize crystal dissolution, some exchange of protein into the surrounding buffer is inevitable and could explain the observation of two polarization timescales. However, we consider this is a less likely explanation given the differences observed for 20 mM radical vs. 40 mM radical.

The optimal recycling delays calculated from the buildup curves were 67 s and 497 s for 40 mM and 20 mM trityl OX063, respectively. Overall, the 40 mM trityl OX063 provided better SNR per unit time. More importantly, the SNR per unit time for a DPMAS spectrum for the sample containing 40 mM trityl OX063 was 60% better than the optimal DNP CPMAS spectrum for the sample containing 20 mM AMUPol. We note that in other protein samples where the AMUPol concentration has been extensively optimized, the best results are typically observed at ~10 mM AMUPol for 600 MHz MAS-DNP. However, we chose 20 mM AMUPol for comparison in this study to match the radical concentration. Thus, it is possible that with a more optimal AMUPol concentration the SNR per unit time may be equivalent or even better than that observed for trityl OX063. Nonetheless, we were able to achieve significant polarization using a narrow line monoradical suggesting new directions for achieving optimal DNP at high magnetic fields (Fig. 4). In comparing the MAS-DNP NMR spectra for the two radicals (Fig. 5), we note that the DPMAS spectrum for the trityl-containing sample has a significantly higher relative intensity for the resonances at 240–250 ppm compared to the CPMAS spectrum for the AMUPol-containing sample. This region corresponds to histidine nitrogens in the TS enzyme which are not protonated. This highlights possible approaches for direct polarization of low gamma nuclei, particularly those which are not protonated and thus more difficult to enhance with a biradical and CPMAS approach. Q3

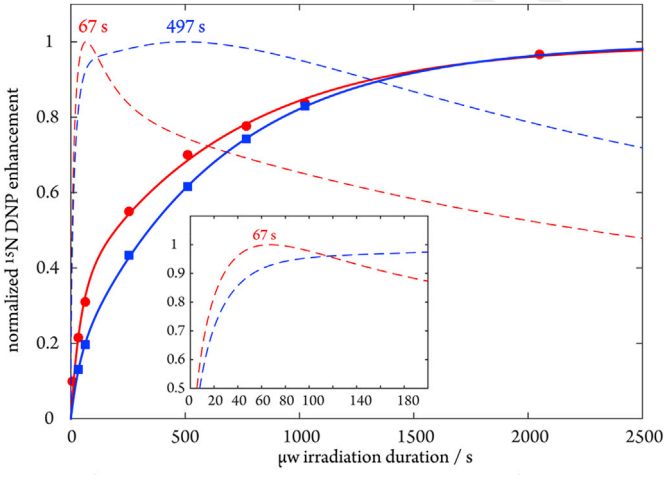

Fig. 3. ^{15}N direct DNP buildup curves and fittings for U-^{15}N TS samples containing 40 mM (red circles) or 20 mM (blue squares) trityl OX063 at a magnetic field strength of 14.0931 T (field corresponding to maximal ^{15}N enhancement for trityl OX063), 11 W of MW power at 395.175 GHz, 98 K and 10 kHz MAS. Solid lines are fits using double exponential functions. Dashed lines are fits of double exponential functions of polarization buildup against square root of buildup times to calculate the optimal repetition rate for maximum SNR per unit time. The optimized buildup times derived from fits are 67 s and 497 s for 40 mM and 20 mM trityl, respectively.

4. Conclusions

In this report we have studied for the first time the potential for direct polarization from a trityl OX063 radical to ^{13}C and ^{15}N nuclei at 14.1 T, corresponding to a magnetic field that is almost three times higher than previous studies [47,60]. Despite the significantly higher magnetic field, our analyses of [^{13}C, ^{15}N] urea samples show a significant polarization gain for both nuclei. We also estimated quenching and depolarization under MAS and recorded DNP enhancement profiles as a function of magnetic field. The DNP enhancement profiles are consistent with a CE mechanism for polarizing ^{15}N nuclei and a mixture of CE and SE mechanisms for polarizing ^{13}C nuclei, although some polarization of ^{15}N via the SE cannot be ruled out. These mechanistic observations are consistent with our estimates of depolarization and quenching effects, with more significant depolarization and bleaching observed for ^{15}N nuclei than for ^{13}C nuclei as would be expected with a predominately CE mechanism for polarizing ^{15}N nuclei and a mixture CE and SE mechanisms for polarizing ^{13}C nuclei.

Finally, we examined the viability of direct polarization for enhancing ^{15}N sensitivity in a biologically relevant sample. Remarkably, the time

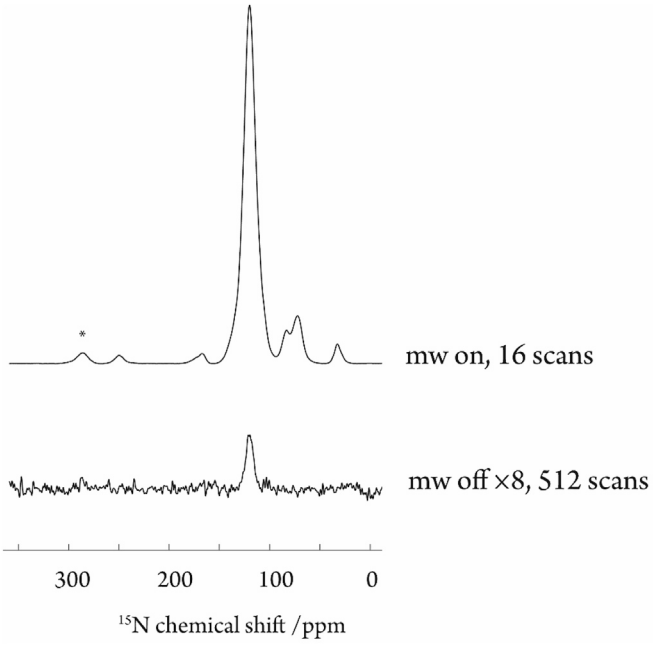

Fig. 4. DPMAS ^{15}N spectra with and without microwaves for ^{15}N-enriched Tryptophan Synthase sample containing 40 mM trityl OX063. A recycle delay time of 176 s was used for both experiments. Spectra acquired at 14.1 T with 10 kHz MAS at 98 K. Input MW power was set to 11 W at 395.175 GHz for the MW-on experiment.

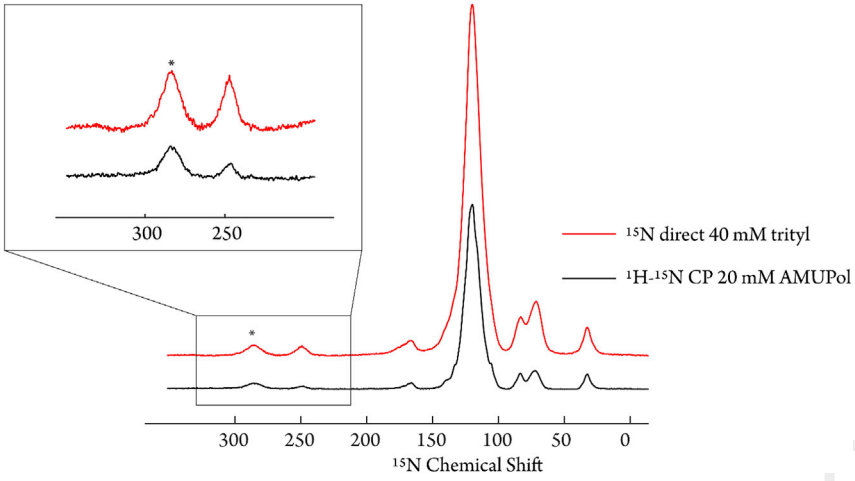

Fig. 5. Comparison ^{15}N spectra for ^{15}N-enriched Tryptophan synthase collected using CPMAS and 20 mM AMUPol (black spectrum) vs DPMAS and 40 mM trityl OX063 (red spectrum). CPMAS and DPMAS spectra were collected with acquisition times of 6372 s (2048 scans) and 6926 s (128 scans), respectively, and scaled for their relative acquisition times. Spectra acquired at 14.1 T with 10 kHz MAS at 98 K. Input MW power was set to 11 W at 395.175 GHz. For direct ^{15}N MAS experiment, the recycle delay was set to 54 s for each transient. A larger relative enhancement is observed in the DPMAS spectrum at 240–250 ppm corresponding to unprotonated ^{15}N moieties.

unit sensitivity was on par and even slightly better when comparing 40 mM trityl OX063 and DPMAS spectra to 20 mM AMUPol and CPMAS spectra. This is an unexpected result considering the exceedingly long time required to directly polarize ^{15}N spins. Thus, the direct polarization using trityl radicals can be considered even for high magnetic field applications and one may expect further considerable improvements with the development of trityl-based biradicals.

Notes

The authors declare no competing financial interest.

Acknowledgements

This research was supported by NIH P41 GM122698 to J.R. Long and NIH R01 GM097569 and NSF CHE-1710671 to L.J. Mueller. The gyrotron was purchased through an NSF MRI award, CHE-1229170, and the magnet and NMR console were purchased through NIH S10 OD018519. A portion of this work was performed at the National High Magnetic Field Laboratory, which is supported by National Science Foundation Cooperative Agreement Nos. DMR-1157490 and DMR-1644779 and the State of Florida.

Appendix A. Supplementary data

Supplementary data to this article can be found online at https://doi.org/10.1016/j.ssnmr.2019.03.009.

References

[1] A. Lesage, M. Lelli, D. Gajan, M.A. Caporini, V. Vitzthum, P. Miéville, J. Alauzun, A. Roussey, C. Thieuleux, A. Mehdi, G. Bodenhausen, C. Coperet, L. Emsley, Surface enhanced NMR spectroscopy by dynamic nuclear polarization, J. Am. Chem. Soc. 132 (2010) 15459–15461, https://doi.org/10.1021/ja104771z.

[2] V. Vitzthum, P. Miéville, D. Carnevale, M.A. Caporini, D. Gajan, C. Copéret, M. Lelli, A. Zagdoun, A.J. Rossini, A. Lesage, L. Emsley, G. Bodenhausen, Dynamic nuclear polarization of quadrupolar nuclei using cross polarization from protons: surface-enhanced aluminium-27 NMR, Chem. Commun. 48 (2012) 1988, https://doi.org/10.1039/c2cc15905h.

[3] D. Lee, H. Takahashi, A.S.L. Thankamony, J.-P. Dacquin, M. Bardet, O. Lafon, G. De Paëpe, Enhanced solid-state NMR correlation spectroscopy of quadrupolar nuclei using dynamic nuclear polarization, J. Am. Chem. Soc. 134 (2012) 18491–18494, https://doi.org/10.1021/ja307755t.

[4] D. Lee, N.T. Duong, O. Lafon, G. De Paëpe, Primostrato solid-state NMR enhanced by dynamic nuclear polarization: pentacoordinated Al3+ ions are only located at the surface of hydrated γ-alumina, J. Phys. Chem. C 118 (2014) 25065–25076, https://doi.org/10.1021/jp508009x.

[5] F.A. Perras, T. Kobayashi, M. Pruski, Natural abundance 17O DNP two-dimensional and surface enhanced NMR spectroscopy, J. Am. Chem. Soc. (2015), https://doi.org/10.1021/jacs.5b03905, 150622115706000.

[6] T. Kobayashi, I.I. Slowing, M. Pruski, Measuring long-range 13 C– 13 C correlations on a surface under natural abundance using dynamic nuclear polarization-enhanced solid-state nuclear magnetic resonance, J. Phys. Chem. C (2017), https://doi.org/10.1021/acs.jpcc.7b08841 acs.jpcc.7b08841.

[7] E.J. Koers, E. a W. van der Cruijsen, M. Rosay, M. Weingarth, A. Prokofyev, C. Sauvée, O. Ouari, J. van der Zwan, O. Pongs, P. Tordo, W.E. Maas, M. Baldus, NMR-based structural biology enhanced by dynamic nuclear polarization at high magnetic field, J. Biomol. NMR 60 (2014) 157–168, https://doi.org/10.1007/s10858-014-9865-8.

[8] P. Fricke, D. Mance, V. Chevelkov, K. Giller, S. Becker, M. Baldus, A. Lange, High resolution observed in 800 MHz DNP spectra of extremely rigid type III secretion needles, J. Biomol. NMR 65 (2016) 121–126, https://doi.org/10.1007/s10858-016-0044-y.

[9] M.R. Elkins, I.V. Sergeyev, M. Hong, Determining cholesterol binding to membrane proteins by cholesterol 13 C labeling in yeast and dynamic nuclear polarization NMR, J. Am. Chem. Soc. 140 (2018) 15437–15449, https://doi.org/10.1021/jacs.8b09658.

[10] S.Y. Liao, M. Lee, T. Wang, I.V. Sergeyev, M. Hong, Efficient DNP NMR of membrane proteins: sample preparation protocols, sensitivity, and radical location, J. Biomol. NMR 64 (2016) 223–237, https://doi.org/10.1007/s10858-016-0023-3.

[11] E.J. Koers, M.P. López-Deber, M. Weingarth, D. Nand, D.T. Hickman, D. Mlaki Ndao, P. Reis, A. Granet, A. Pfeifer, A. Muhs, M. Baldus, M.P. López-Deber, Dynamic nuclear polarization NMR spectroscopy: revealing multiple conformations in lipid-anchored Peptide vaccines, Angew Chem. Int. Ed. Engl. 52 (2013) 10905–10908, https://doi.org/10.1002/anie.201303374.

[12] Q.Z. Ni, T.V. Can, E. Daviso, M. Belenky, R.G. Griffin, J. Herzfeld, Primary transfer step in the light-driven ion pump bacteriorhodopsin: an irreversible U-turn revealed by dynamic nuclear polarization-enhanced magic angle spinning NMR, J. Am. Chem. Soc. 140 (2018) 4085–4091, https://doi.org/10.1021/jacs.8b00022.

[13] K.K. Frederick, V.K. Michaelis, B. Corzilius, T. Ong, A.C. Jacavone, R.G. Griffin, S. Lindquist, Sensitivity-Enhanced NMR reveals alterations in protein structure by cellular milieus, Cell 163 (2015) 620–628, https://doi.org/10.1016/j.cell.2015.09.024.

[14] H. Takahashi, S. Hediger, G. De Paëpe, Matrix-free dynamic nuclear polarization enables solid-state NMR 13C-13C correlation spectroscopy of proteins at natural isotopic abundance, Chem. Commun. 49 (2013) 9479–9481, https://doi.org/10.1039/c3cc45195j.

[15] K. Märker, S. Paul, C. Fernández-de-Alba, D. Lee, J.-M. Mouesca, S. Hediger, G. De Paëpe, Welcoming natural isotopic abundance in solid-state NMR: probing π-stacking and supramolecular structure of organic nanoassemblies using DNP, Chem. Sci. 8 (2017) 974–987, https://doi.org/10.1039/C6SC02709A.

[16] A.N. Smith, K. Märker, T. Piretra, J.C. Boatz, I. Matlahov, R. Kodali, S. Hediger, P.C.A. van der Wel, G. De Paëpe, Structural fingerprinting of protein aggregates by dynamic nuclear polarization-enhanced solid-state NMR at natural isotopic abundance, J. Am. Chem. Soc. 140 (2018) 14576–14580, https://doi.org/10.1021/jacs.8b09002.

[17] F.A. Perras, U. Chaudhary, I.I. Slowing, M. Pruski, Probing surface hydrogen bonding and dynamics by natural abundance, multidimensional, 17 O DNP-NMR spectroscopy, J. Phys. Chem. C 120 (2016) 11535–11544, https://doi.org/10.1021/acs.jpcc.6b02579.

[18] A. Kirui, Z. Ling, X. Kang, M.C. Dickwella Widanage, F. Mentink-Vigier, A.D. French, T. Wang, Atomic resolution of cotton cellulose structure enabled by dynamic nuclear polarization solid-state NMR, Cellulose 6 (2018), https://doi.org/10.1007/s10570-018-2095-6.

[19] G. Mollica, M. Dekhil, F. Ziarelli, P. Thureau, S. Viel, Quantitative structural constraints for organic powders at natural isotopic abundance using dynamic nuclear polarization solid-state NMR spectroscopy, Angew. Chem. Int. Ed. 54 (2015) 6028–6031, https://doi.org/10.1002/anie.201501172.

[20] D.A. Hall, D.C. Maus, G.J. Gerfen, S.J. Inati, L.R. Becerra, F.W. Dahlquist, R.G. Griffin, Polarization-enhanced NMR spectroscopy of biomolecules in frozen

solution, Science 276 (1997) 930–932, https://doi.org/10.1126/science.276.5314.930.
[21] M. Rosay, L. Tometich, S. Pawsey, R. Bader, R. Schauwecker, M. Blank, P.M. Borchard, S.R. Cauffman, K.L. Felch, R.T. Weber, R.J. Temkin, R.G. Griffin, W.E. Maas, Solid-state dynamic nuclear polarization at 263 GHz: spectrometer design and experimental results, Phys. Chem. Chem. Phys. 12 (2010) 5850, https://doi.org/10.1039/c003685b.
[22] K.-N. Hu, H. Yu, T.M. Swager, R.G. Griffin, Dynamic nuclear polarization with biradicals, J. Am. Chem. Soc. 126 (2004) 10844–10845, https://doi.org/10.1021/ja039749a.
[23] K.R. Thurber, R. Tycko, Theory for cross effect dynamic nuclear polarization under magic-angle spinning in solid state nuclear magnetic resonance: the importance of level crossings, J. Chem. Phys. 137 (2012), 084508, https://doi.org/10.1063/1.4747449.
[24] F. Mentink-Vigier, U. Akbey, Y. Hovav, S. Vega, H. Oschkinat, A. Feintuch, Fast passage dynamic nuclear polarization on rotating solids, J. Magn. Reson. 224 (2012) 13–21, https://doi.org/10.1016/j.jmr.2012.08.013.
[25] E. Stejskal, J. Schaefer, J. Waugh, Magic-angle spinning and polarization transfer in proton-enhanced NMR, J. Magn. Reson. 28 (1977) 105–112, https://doi.org/10.1016/0022-2364(77)90260-8.
[26] A. Pines, M.G. Gibby, J.S. Waugh, Proton-enhanced NMR of dilute spins in solids, J. Chem. Phys. 59 (1973) 569–590, https://doi.org/10.1063/1.1680061.
[27] R.L. Johnson, K. Schmidt-Rohr, Quantitative solid-state 13C NMR with signal enhancement by multiple cross polarization, J. Magn. Reson. (2013), https://doi.org/10.1016/j.jmr.2013.11.009.
[28] S. Björgvinsdóttir, B.J. Walder, A. Pinon, L. Emsley, Bulk nuclear hyperpolarization of inorganic solids by relay from the surface, J. Am. Chem. Soc. 140 (2018) 7946–7951, https://doi.org/10.1021/jacs.8b03883.
[29] C. Sauvée, M. Rosay, G. Casano, F. Aussenac, R.T. Weber, O. Ouari, P. Tordo, Highly efficient, water-soluble polarizing agents for dynamic nuclear polarization at high frequency, Angew. Chem. Int. Ed. 52 (2013) 10858–10861, https://doi.org/10.1002/anie.201304657.
[30] D.J. Kubicki, G. Casano, M. Schwarzwälder, S. Abel, C. Sauvée, K. Ganesan, M. Yulikov, A.J. Rossini, G. Jeschke, C. Copéret, A. Lesage, P. Tordo, O. Ouari, L. Emsley, Rational design of dinitroxide biradicals for efficient cross-effect dynamic nuclear polarization, Chem. Sci. 7 (2016) 550–558, https://doi.org/10.1039/C5SC02921J.
[31] C. Sauvée, G. Casano, S. Abel, A. Rockenbauer, D. Akhmetzyanov, H. Karoui, D. Siri, F. Aussenac, W. Maas, R.T. Weber, T.F. Prisner, M. Rosay, P. Tordo, O. Ouari, Tailoring of polarizing agents in the bTurea series for cross-effect dynamic nuclear polarization in aqueous media, Chem. Eur J. 22 (2016) 5598–5606, https://doi.org/10.1002/chem.201504693.
[32] G. Mathies, M.A. Caporini, V.K. Michaelis, Y. Liu, K.-N. Hu, D. Mance, J.L. Zweier, M. Rosay, M. Baldus, R.G. Griffin, Efficient dynamic nuclear polarization at 800 MHz/527 GHz with trityl-nitroxide biradicals, Angew. Chem. Int. Ed. 127 (2015) 11936–11940, https://doi.org/10.1002/ange.201504292.
[33] F. Mentink-Vigier, I. Marin-Montesinos, A.P. Jagtap, T. Halbritter, J. van Tol, S. Hediger, D. Lee, S.T. Sigurdsson, G. De Paëpe, Computationally assisted design of polarizing agents for dynamic nuclear polarization enhanced NMR: the AsymPol family, J. Am. Chem. Soc. 140 (2018) 11013–11019, https://doi.org/10.1021/jacs.8b04911.
[34] C. Fernández-de-Alba, H. Takahashi, A. Richard, Y. Chenavier, L. Dubois, V. Maurel, D. Lee, S. Hediger, G. De Paëpe, Matrix-free DNP-enhanced NMR spectroscopy of liposomes using a lipid-anchored biradical, Chem. Eur J. 21 (2015) 4512–4517, https://doi.org/10.1002/chem.201404588.
[35] E.S. Salnikov, S. Abel, G. Karthikeyan, H. Karoui, F. Aussenac, P. Tordo, B. Bechinger, O. Ouari, Dynamic nuclear polarization/solid-state NMR spectroscopy of membrane polypeptides: free-radical optimization for matrix-free lipid bilayer samples, ChemPhysChem 18 (2017) 2103–2113, https://doi.org/10.1002/cphc.201700389.
[36] A.N. Smith, U.T. Twahir, T. Dubroca, G.E. Fanucci, J.R. Long, Molecular rationale for improved dynamic nuclear polarization of biomembranes, J. Phys. Chem. B 120 (2016) 7880–7888, https://doi.org/10.1021/acs.jpcb.6b02885.
[37] M. a. Voinov, D.B. Good, M.E. Ward, S. Milikisiyants, A. Marek, M.A. Caporini, M. Rosay, R. a. Munro, M. Ljumovic, L.S. Brown, V. Ladizhansky, A.I. Smirnov, Cysteine-specific labeling of proteins with a nitroxide biradical for dynamic nuclear polarization NMR, J. Phys. Chem. B 119 (2015) 10180–10190, https://doi.org/10.1021/acs.jpcb.5b05230.
[38] M. Lelli, S.R. Chaudhari, D. Gajan, G. Casano, A.J. Rossini, O. Ouari, P. Tordo, A. Lesage, L. Emsley, Solid-state dynamic nuclear polarization at 9.4 and 18.8 T from 100 K to room temperature, J. Am. Chem. Soc. 137 (2015) 14558–14561, https://doi.org/10.1021/jacs.5b08423.
[39] D. Mance, P. Gast, M. Huber, M. Baldus, K.L. Ivanov, The magnetic field dependence of cross-effect dynamic nuclear polarization under magic angle spinning, J. Chem. Phys. 142 (2015) 234201, https://doi.org/10.1063/1.4922219.
[40] F. Mentink-Vigier, S. Paul, D. Lee, A. Feintuch, S. Hediger, S. Vega, G. De Paëpe, Nuclear depolarization and absolute sensitivity in magic-angle spinning cross effect dynamic nuclear polarization, Phys. Chem. Chem. Phys. 17 (2015) 21824–21836, https://doi.org/10.1039/C5CP03457D.
[41] S. Björgvinsdóttir, B.J. Walder, A. Pinon, J. Reddy Yarava, L. Emsley, DNP enhanced NMR with flip-back recovery, J. Magn. Reson. (2018), https://doi.org/10.1016/j.jmr.2018.01.017.
[42] F. Mentink-Vigier, U. Akbey, H. Oschkinat, S. Vega, A. Feintuch, Theoretical aspects of magic angle spinning - dynamic nuclear polarization, J. Magn. Reson. 258 (2015) 102–120, https://doi.org/10.1016/j.jmr.2015.07.001.
[43] F. Mentink-Vigier, S. Vega, G. De Paëpe, Fast and accurate MAS–DNP simulations of large spin ensembles, Phys. Chem. Chem. Phys. 19 (2017) 3506–3522, https://doi.org/10.1039/C6CP07881H.
[44] O. Lafon, M. Rosay, F. Aussenac, X. Lu, J. Trébosc, O. Cristini, C. Kinowski, N. Touati, H. Vezin, J.P. Amoureux, Beyond the silica surface by direct silicon-29 dynamic nuclear polarization, Angew. Chem. Int. Ed. 50 (2011) 8367–8370, https://doi.org/10.1002/anie.201101841.
[45] F.A. Perras, K.C. Boteju, I.I. Slowing, A.D. Sadow, M. Pruski, Direct 17O dynamic nuclear polarization of single-site heterogeneous catalysts, Chem. Commun. (2018) 3–8, https://doi.org/10.1039/C8CC00293B.
[46] M. Kaushik, M. Qi, A. Godt, B. Corzilius, Bis-gadolinium complexes for solid effect and cross effect dynamic nuclear polarization, Angew. Chem. Int. Ed. 56 (2017) 4295–4299, https://doi.org/10.1002/anie.201612388.
[47] V.K. Michaelis, B. Corzilius, A.A. Smith, R.G. Griffin, Dynamic nuclear polarization of 17 O: direct polarization, J. Phys. Chem. B 117 (2013) 14894–14906, https://doi.org/10.1021/jp408440z.
[48] T. Chakrabrty, N. Goldin, A. Feintuch, L. Houben, M. Leskes, Paramagnetic metal ion dopants as polarization agents for DNP NMR spectroscopy in inorganic solids, ChemPhysChem 5 (2018) 644–656, https://doi.org/10.1002/cphc.201800462.
[49] N.M. Loening, M. Rosay, V. Weis, R.G. Griffin, Solution-state dynamic nuclear polarization at high magnetic field, J. Am. Chem. Soc. 124 (2002) 8808–8809, https://doi.org/10.1021/ja026660g.
[50] T. Maly, L.B. Andreas, A.A. Smith, R.G. Griffin, 2H-DNP-enhanced 2H-13C solid-state NMR correlation spectroscopy, Phys. Chem. Chem. Phys. 12 (2010) 5872–5878, https://doi.org/10.1039/c003705b.
[51] T. Maly, A.-F. Miller, R.G. Griffin, In situ high-field dynamic nuclear polarization-direct and indirect polarization of 13C nuclei, ChemPhysChem 11 (2010) 999–1001, https://doi.org/10.1002/cphc.200900908.
[52] T. Wolf, S. Kumar, H. Singh, T. Chakrabarty, F. Aussenac, A.I. Frenkel, D.T. Major, M. Leskes, Endogenous dynamic nuclear polarization for natural abundance 17 O and lithium NMR in the bulk of inorganic solids, J. Am. Chem. Soc. 141 (2019) 451–462, https://doi.org/10.1021/jacs.8b11015.
[53] M. Kaushik, T. Bahrenberg, T.V. Can, M.A. Caporini, R. Silvers, J. Heiliger, A.A. Smith, H. Schwalbe, R.G. Griffin, B. Corzilius, Gd(III) and Mn(II) complexes for dynamic nuclear polarization: small molecular chelate polarizing agents and applications with site-directed spin labeling of proteins, Phys. Chem. Chem. Phys. (2016), https://doi.org/10.1039/C6CP04623A.
[54] Y.M. Huang, W. You, B.G. Caulkins, M.F. Dunn, L.J. Mueller, C.A. Chang, Protonation states and catalysis: molecular dynamics studies of intermediates in tryptophan synthase, Protein Sci. 25 (2016) 166–183, https://doi.org/10.1002/pro.2709.
[55] B.G. Caulkins, B. Bastin, C. Yang, T.J. Neubauer, R.P. Young, E. Hilario, Y.M. Huang, C.A. Chang, L. Fan, M.F. Dunn, M.J. Marsella, L.J. Mueller, Protonation states of the tryptophan synthase internal aldimine active site from solid-state NMR spectroscopy: direct observation of the protonated schiff base linkage to pyridoxal-5′-phosphate, J. Am. Chem. Soc. 136 (2014) 12824–12827, https://doi.org/10.1021/ja506267d.
[56] S. Stoll, A. Schweiger, EasySpin, a comprehensive software package for spectral simulation and analysis in EPR, J. Magn. Reson. 178 (2006) 42–55, https://doi.org/10.1016/j.jmr.2005.08.013.
[57] L. Lumata, Z. Kovacs, A.D. Sherry, C. Malloy, S. Hill, J. van Tol, L. Yu, L. Song, M.E. Merritt, Electron spin resonance studies of trityl OX063 at a concentration optimal for DNP, Phys. Chem. Chem. Phys. 15 (2013) 9800, https://doi.org/10.1039/c3cp50186h.
[58] T. Dubroca, A.N. Smith, K.J. Pike, S. Froud, R. Wylde, B. Trociewitz, J. McKay, F. Mentink-Vigier, J. van Tol, S. Wi, W. Brey, J.R. Long, L. Frydman, S. Hill, A quasi-optical and corrugated waveguide microwave transmission system for simultaneous dynamic nuclear polarization NMR on two separate 14.1 T spectrometers, J. Magn. Reson. 289 (2018) 35–44, https://doi.org/10.1016/j.jmr.2018.01.015.
[59] A.J. Rossini, A. Zagdoun, M. Lelli, D. Gajan, F. Rascón, M. Rosay, W.E. Maas, C. Copéret, A. Lesage, L. Emsley, One hundred fold overall sensitivity enhancements for Silicon-29 NMR spectroscopy of surfaces by dynamic nuclear polarization with CPMG acquisition, Chem. Sci. 3 (2012) 108–115, https://doi.org/10.1039/C1SC00550B.
[60] V.K. Michaelis, A.A. Smith, B. Corzilius, O. Haze, T.M. Swager, R.G. Griffin, High-field 13C dynamic nuclear polarization with a radical mixture, J. Am. Chem. Soc. 135 (2013) 2935–2938, https://doi.org/10.1021/ja312265x.
[61] K.R. Thurber, R. Tycko, Low-temperature dynamic nuclear polarization with helium-cooled samples and nitrogen-driven magic-angle spinning, J. Magn. Reson. 264 (2016) 99–106, https://doi.org/10.1016/j.jmr.2016.01.011.
[62] M. Blank, K.L. Felch, Millimeter-wave Sources for DNP-NMR 7 (2018) 155–166, https://doi.org/10.1002/9780470034590.emrstm1582.
[63] T.F. Kemp, H.R.W. Dannatt, N.S. Barrow, A. Watts, S.P. Brown, M.E. Newton, R. Dupree, Dynamic nuclear polarization enhanced NMR at 187GHz/284MHz using an extended interaction klystron amplifier, J. Magn. Reson. 265 (2016) 77–82, https://doi.org/10.1016/j.jmr.2016.01.021.
[64] E. Hilario, B.G. Caulkins, Y.-M.M. Huang, W. You, C.-E.A. Chang, L.J. Mueller, M.F. Dunn, L. Fan, Visualizing the tunnel in tryptophan synthase with crystallography: insights into a selective filter for accommodating indole and rejecting water, Biochim. Biophys. Acta Protein Proteonomics 1864 (2016) 268–279, https://doi.org/10.1016/j.bbapap.2015.12.006.
[65] O. Lafon, A.S.L. Thankamony, M. Rosay, F. Aussenac, X. Lu, J. Trébosc, V. Bout-Roumazeilles, H. Vezin, J.P. Amoureux, Indirect and direct 29Si dynamic nuclear polarization of dispersed nanoparticles, Chem. Commun. (J. Chem. Soc. Sect. D) 49 (2013) 2864–2866, https://doi.org/10.1039/c2cc36170a.
[66] A. Pinon, J. Schlagnitweit, P. Berruyer, A.J. Rossini, M. Lelli, E. Socie, M. Tang, T. Pham, A. Lesage, S. Schantz, L. Emsley, Measuring nano- to microstructures from

relayed dynamic nuclear polarization NMR, J. Phys. Chem. C (2017), https://doi.org/10.1021/acs.jpcc.7b04438 acs.jpcc.7b04438.
[67] A.J. Rossini, A. Zagdoun, F. Hegner, M. Schwarzwälder, D. Gajan, C. Copéret, A. Lesage, L. Emsley, Dynamic nuclear polarization NMR spectroscopy of microcrystalline solids, J. Am. Chem. Soc. 134 (2012) 16899–16908, https://doi.org/10.1021/ja308135r.

Xiaoling Wang[a,1], Bethany G. Caulkins[b], Gwladys Riviere[c], Leonard J. Mueller[b], Frederic Mentink-Vigier[a], Joanna R. Long[a,c,*]
[a] *National High Magnetic Field Laboratory, Tallahassee, FL, 32310, USA*
[b] *Department of Chemistry, University of California Riverside, Riverside, CA, 92521, USA*
[c] *Department of Biochemistry and Molecular Biology and McKnight Brain Institute, University of Florida, Gainesville, FL, 32610-0245, USA*

[*] Corresponding author. National High Magnetic Field Laboratory, Tallahassee, FL, 32310, USA.
E-mail address: jrlong@mbi.ufl.edu (J.R. Long).

[1] Current address: Department of Physics, University of California Santa Barbara, Santa Barbara, California, 93160.